Analysis of the turbulent boundary layer on a flat plate at M=6÷8.8 with the use of NERAT-2D code and algebraic turbulence models

IOP Conf. Series: Journal of Physics: Conf. Series **1009** (2018) 012016 doi:10.1088/1742-6596/1009/1/012016

Analysis of the turbulent boundary layer on a flat plate at M=6÷8.8 with the use of NERAT-2D code and algebraic turbulence models

S T Surzhikov

Ishlinsky Institute for Problems in Mechanics RAS,Vernadsky prospekt 101(1), Moscow, 119526, Russia
Moscow Institute of Physics and Technology (State University), 9 Institutskiy per., Dolgoprudny, Moscow Region, 141701, Russia
Dukhov All-Russian Scientific Research Institute of Automatics, Moscow, Russia

surg@ipmnet.ru

Abstract. Experimental data on heat transfer of supersonic air flows to flat plate, which were analysed by Dilley A.D [NASA/CR-2001-210837, 2001], are compared for Mach numbers $M=6\div8.8$ with the calculated data obtained using the Navier – Stokes flow model in conjunction with the analytical models of turbulent mixing of the Prandtl mixing length and the Baldwin-Lomax model. In the paper, the author's computer code NERAT-2D was used for numerical study.

1. Introduction

One of the key tasks of hypersonic aerothermodynamics is the heating of the surface of a high-speed aircraft.The primary problems of external aerothermodynamics are:

- heating blunted edges of hypersonic aircrafts, air intakes as well as steering controls;
- local heating of the surface in the interaction of incident shock waves with boundary layers;
- local heating in the laminar-turbulent transition (LTP) and turbulent heating of the developed surface.

A detailed calculation of the thermal regimes of the region of turbulent motion and the LTP zone in hypersonic flow past a flat plate was carried out in [1]. The studied speed range was $M=6\div8.8$. The work was carried out as part of the development work of hypersonic aircraft Hyper-X. The advantage of this work is a detailed analysis of three series of experimental data [2– 4] using numerical simulation. For this, the computer code CFL3DE [5] was used, in which three models were realized: the parabalized Navier – Stokes equations, the Navier – Stokes model of a viscous compressed layer, the Euler equations. Algorithmically implemented is an upwind, finite volume flow solver.

An analytical Baldwin – Lomax model [6] was used in [1]. The influence of grids used was studied in detail. The final recommendations of [1] for an adequate description of the experimental data consist in the need to provide a grid detail along the normal to the surface $y^+ < 2$, where $y^+ = \frac{y}{\nu_w}\sqrt{\frac{\tau_w}{\rho_w}}$,

where: y is the coordinate normal to the surface; ν_w is the kinematic viscosity; τ_w is the frictional stress on a surface; ρ_w is the gas density near to surface.

In [1], solutions were obtained for very small sizes of the minimum step along the normal coordinate $\Delta y_1 \sim 0.5\times10^{-4}$ cm (0.5 μm), which corresponded to Reynolds numbers corresponding to the minimal step

$$\mathrm{Re}_{\Delta y_1} = \frac{\rho_\infty V_\infty \Delta y_1}{\mu_\infty} \sim 10$$

In this paper, the author's computer code NERAT-2D [7] is used for numerical analysis of experiments [2– 4] (validation) and comparison with calculation results [1] (verification). This code has been repeatedly tested successfully with the example of physico-chemical aerothermodynamics [8]. Taking into account the urgency of studying the features of the structure of boundary layers at hypersonic velocities of flow above surfaces, experimental [2– 4] and calculated data [1] were chosen to test the work of the NERAT-2D code together with the simplest algebraic model of turbulence.

The problem of convective heating of a flat plate with a sharp edge is classical for aerothermodynamics. This is because the flow model for a plane surface is very versatile with respect to applicability for other types of flows and other geometries. Nevertheless, in spite of the large number of papers devoted to this problem, the problem of convective heat transfer to a plate (or, in a more general formulation, on a surface) for $M > 6$ has not yet been studied sufficiently, in particular regarding the reliable use of turbulent mixing models in aerothermodynamic computer codes .

This problem has been studied most extensively in experimental and computational studies, the results of which have been generalized in [9– 11]. Approximate analytical solutions are also obtained for this problem. On the basis of these solutions and experimental data, approximate semi empirical relationships are proposed, which have become widely used in practical aerothermodynamics. These correlations have been repeatedly tested in a wide range of applications, and they underlie the sectoral techniques used with a high degree of reliability in the profile aerospace organizations. Multiple confirmation of the reliability of the calculated data resulted in the fact that modern computational models are primarily tested by comparing precisely with these correlations.

Despite the convincing results of the development of the theory of the boundary layer for a flat plate, there are a limited number of publications on the structure of the boundary layer at hypersonic flow velocities, in particular, flow regimes with a laminar-turbulent transition.

2. Approximate correlations based on criterial relations of boundary layer theory

The most widely used model of heat transfer is based on the introduction of an effective heat transfer coefficient [9].

For a *laminar* boundary layer

$$q_w = \left(\frac{\alpha_l}{c_p}\right)\left(H_e - h_w\right), \tag{1}$$

$$H_e = h_\delta + \frac{1}{2}\kappa V_\delta^2, \tag{2}$$

$$\left(\frac{\alpha_l}{c_p}\right) = 0.332\,\mathrm{Pr}_w^{-2/3}\rho_* V_\delta \sqrt{\frac{(2\nu+1)\,\mu_*}{\rho_* V_\delta x}}, \tag{3}$$

where q_w is the convective heat flux density; $\left(\alpha_l/c_p\right)$ is the effective heat transfer coefficient for a laminar boundary layer; H_e, h_δ are the adiabatic wall enthalpy and thermodynamic enthalpy, $h = e + \left(p/s\right)$; e is the specific internal energy.

To calculate the density of a convective heat flux for a laminar flow past a plate ($\nu = 0$) or an acute cone ($\nu = 1$), the following algorithm can be used:

1) First, the initial flow data is specified. For example, in the case under consideration, based on [1] one can use

$$c_p = 10^7 \text{ erg/(g×K)},\ M_\Sigma = 29 \text{ g/mole},\ T_\infty = T_\delta = 65.04 \text{ K},\ V_\infty = V_\delta = 9.696\times10^4 \text{ cm/s},$$

$\gamma = 1.4$, $R_0 = 8.3145\times10^7$ erg/(mole×K), Mach number $\mathrm{M}_\delta = 6$, $T_w = 320$ K, $\mathrm{Pr}_w = \mu_w c_p / \lambda_w$, $h_w = c_\rho T_w$,

where indices δ and w indicate the flow parameters at the outer boundary of the boundary layer and at the surface.

2) Using these data, the enthalpy, temperature and density are calculated:

$$h_\delta = c_\rho T_\delta,\ h_w = c_p T_w,\ \ h_* = \frac{1}{2}\left(h_\delta + h_w\right) + 0.11\sqrt{\mathrm{Pr}_w}V_\delta^2,\ \ T_* = \frac{h_*}{c_p},\ \ \rho_* = \frac{p_\delta M_\Sigma}{R_0 T_*}$$

The viscosity is determined by Sutherland's formula

$$\mu_* = C_1 \frac{T_*^{3/2}}{T_* + 110.4},\quad C_1 = 1.458\times10^{-5} \text{ g/(cm×s×K}^{1|2}\text{)}$$

3) Then calculations of q_w are made at each section in x according to formulas (1)–(3).

The friction stress was also calculated

$$\tau_w = 0.332\rho_* V_\delta^2 \sqrt{\frac{(2\nu+1)\mu_*}{\rho_* V_\delta x}} \tag{4}$$

The density of the convective heat flux and the frictional stress in the *turbulent* boundary layer is determined in an analogous sequence by the formulas

$$q_w = \left(\frac{\alpha_t}{c_p}\right)\left(H_e - h_w\right) = 0.0296\,\mathrm{Pr}^{-0.6} K_* \rho_\delta \mathrm{Re}_\delta^{-0.2}\left(H_e - h_w\right), \tag{5}$$

$$\tau_w = 0.0296 K_* \rho_\delta V_\delta^2 \mathrm{Re}_\delta^{-0.2}, \tag{6}$$

$$K_* = \left(\frac{\rho_*}{\rho_\delta}\right)^{0.8}\left(\frac{\mu_*}{\mu_\delta}\right)^{0.2},$$

$$\mathrm{Re}_\delta = \frac{\rho_\delta V_\delta x}{\mu_\delta},\ H_e = h_\delta + \frac{1}{2}\kappa V_\delta^2,\ \kappa = \mathrm{Pr}^{1/3}$$

The characteristic parameters ρ_* and μ_* are calculated using T_*, which, in its turn, is calculated with *reference* enthalpy

$$h_* = \frac{1}{2}\left(h_\delta + h_w\right) + 0.22\left(H_e - h_\delta\right) = \frac{1}{2}\left(H_\delta + H_w\right) - \left(\frac{1}{2} - 0.22\kappa\right)\frac{V_\delta^2}{2} = \frac{1}{2}\left(h_\delta + h_w\right) + \frac{0.22}{2}\kappa V_\delta^2,$$

$$H_\delta = h_\delta + \frac{V_\delta^2}{2}$$

After calculating the surface friction stress and the density of the convective heat flux, the dimensionless friction and heat transfer coefficients (Stanton numbers) are determined

$$C_f = \frac{\tau_w}{0.5\rho_\delta V_\infty^2}, \tag{7}$$

$$\mathrm{St} = \frac{q_w}{\rho_\delta V_\delta \left(H_e - h_w\right)} = \frac{q_w}{0.5\rho_\delta V_\delta^3} \tag{8}$$

3. Calculating model of surface flow based on the Navier – Stokes equations

The dynamics of a viscous, heat-conducting gas is calculated using the Navier – Stokes equations in a two-dimensional formulation. The calculated region includes the flow field in the undisturbed flow, behind the front of the shock wave formed behind the sharp edge of the streamlined plate and above its surface.

The initial system of equations is formulated as follows:

$$\frac{\partial \rho}{\partial t} + \mathrm{div}(\rho \mathbf{V}) = 0, \tag{9}$$

$$\frac{\partial \rho u}{\partial t} + \mathrm{div}\left(\rho u \mathbf{V}\right) = -\frac{\partial p}{\partial x} - \frac{2}{3}\frac{\partial}{\partial x}\left(\mu_{eff}\,\mathrm{div}\mathbf{V}\right) + \frac{\partial}{\partial y}\left[\mu_{eff}\left(\frac{\partial u}{\partial y} + \frac{\partial v}{\partial x}\right)\right] + 2\frac{\partial}{\partial x}\left(\mu_{eff}\frac{\partial u}{\partial x}\right), \tag{10}$$

$$\frac{\partial \rho v}{\partial t} + \mathrm{div}\left(\rho v \mathbf{V}\right) = -\frac{\partial p}{\partial y} - \frac{2}{3}\frac{\partial}{\partial y}\left(\mu_{eff}\,\mathrm{div}\mathbf{V}\right) + \frac{\partial}{\partial x}\left[\mu_{eff}\left(\frac{\partial u}{\partial y} + \frac{\partial v}{\partial x}\right)\right] + 2\frac{\partial}{\partial y}\left(\mu_{eff}\frac{\partial v}{\partial y}\right), \tag{11}$$

$$\rho c_p \frac{\partial T}{\partial t} + \rho c_p \mathbf{V}\mathrm{grad}T = \chi\frac{\partial p}{\partial t} + \chi\mathbf{V}\mathrm{grad}p + \mathrm{div}\left(\lambda_{eff}\,\mathrm{grad}T\right) + Q_V, \tag{12}$$

where x, y are the Cartesian coordinates; $\mathbf{V} = (u, v)$ is the flow velocity and its projections on the x and y axes; ρ, p are the density and pressure; $\mu_{eff} = \mu + \mu_t$ is the effective coefficient of viscosity, determined by the Boussinesq hypothesis; μ, μ_t are the dynamic coefficient of viscosity and coefficient of turbulent viscosity; c_p is the specific heat at constant pressure; T is the temperature; λ_{eff}, λ, λ_t are the effective coefficient of thermal conductivity, the coefficients of molecular and turbulent thermal conductivity, which was calculated using the turbulent Prandtl number $\mathrm{Pr}_t = \frac{\mu_t c_p}{\tau_t}$; Q_V is the power of heat release due to dissipative processes and heating from external energy sources.

The energy conservation equation is written here in a non-conservative form with respect to temperature (in the form of the Fourier – Kirchhoff equation). The system of equations (9)– (12) is used in conjunction with the equation of state of an ideal gas

$$p = \rho\frac{R_0}{M_\Sigma}T, \tag{13}$$

where R_0 is the universal gas constant; M_Σ is the molecular weight.

The boundary conditions give the unperturbed incident flow

$$\begin{aligned} &x = 0: \quad u = u_\infty, \quad v = 0, \quad T = T_\infty, \quad p = p_\infty, \quad \rho = \rho_\infty, \\ &y = H: \quad u = u_\infty, \quad v = 0, \quad T = T_\infty, \quad p = p_\infty, \quad \rho = \rho_\infty, \end{aligned} \tag{14}$$

and non-reflecting boundary conditions at the exit from the computational domain

$$x = L: \quad \frac{\partial u}{\partial x} = \frac{\partial v}{\partial x} = \frac{\partial T}{\partial x} = \frac{\partial \rho}{\partial x} = 0 \tag{15}$$

On the surface of a streamlined body, the sticking conditions are formulated as following:

$$x = 0: \qquad u = v = 0 \tag{16}$$

The design scheme of the problem being solved is shown in figure 1.

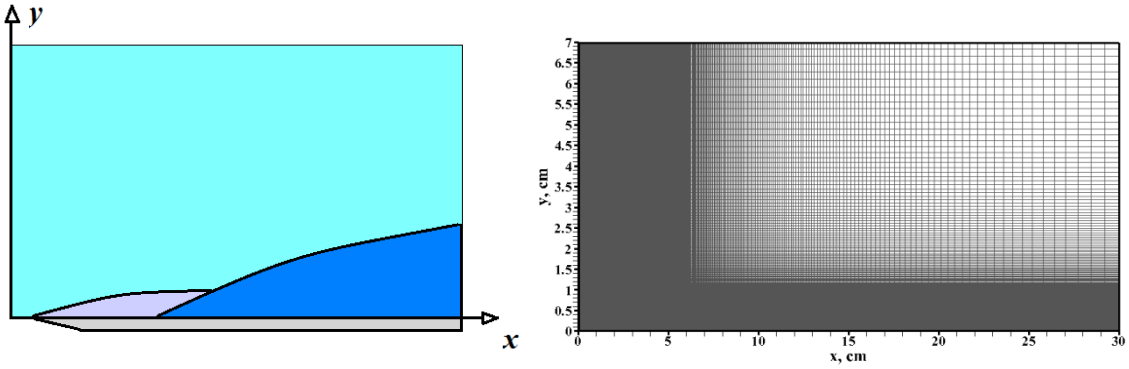

Figure 1. The scheme of the problem (on the left) and the calculated grid 701×401 (along and across the plate).

4. Algebraic models of turbulence

Two algebraic models of turbulent heating and friction of a plane surface were used. The laminar-turbulent transition was determined by specifying the critical Reynolds number

$$\mathrm{Re}_{x,LT} = \frac{\rho_\infty V_\infty x_{LT}}{\mu_\infty},$$

where x_{LT} is the longitudinal coordinate at which the laminar-turbulent transition began.

4.1. The Prandtl turbulent mixing model

This is one of the first and most researched models. In different variations, this model is presented, for example, in [12– 14].

Turbulent viscosity is determined by the well-known phenomenological relationship [15]

$$\mu_t = \rho L_m^2 |\Omega|, \tag{17}$$

where L_m is the mixing length of Prandtl; Ω is the vorticity function.

In the case of the simplest flow near the plate without a pressure gradient in the external flow, it is approximately assumed

$$|\Omega| = \left|\frac{\partial u}{\partial y}\right| \tag{18}$$

A two-layer model is considered, according to which the length of the Prandtl mixing path is determined by the formula:

$$L_m = \begin{cases} L_m^{in} = \kappa y \left[1 - \exp\left(-\dfrac{y^+}{A^+}\right)\right] & \text{at } \dfrac{y}{\delta} < 0.2 \\ L_m^{out} = 0.085\delta & \text{at } \dfrac{y}{\delta} > 0.2, \end{cases} \tag{19}$$

where δ is the thickness of dynamic boundary layer; $\kappa = 0.43$ is the empirical constant; $A^+ = 26$;

$$y^+ = \frac{y}{\nu_w} u_\tau, \quad u_\tau = \sqrt{\frac{\tau_w}{\rho_w}}, \quad \tau_w = \mu_w \left(\frac{\partial u}{\partial y} \right)_w, \tag{20}$$

where ν_w is the kinematic viscosity near the surface.

If we use the relationship between kinematic and dynamic viscosity $\mu = \rho\nu$, then

$$y^+ = \frac{y}{\mu_w} \rho_w u_\tau = \frac{y}{\mu_w} \sqrt{\rho_w \tau_w} = y \sqrt{\frac{\rho_w}{\mu_w} \left(\frac{\partial u}{\partial y} \right)_w} \tag{21}$$

4.2. The Baldwin − Lomax model [6]

A two-layer model is considered. Each layer has its own turbulent viscosity. In the inner layer (closer to the surface)

$$\mu_{t,in} = \kappa \rho y D |\Omega|, \tag{22}$$

where $\kappa = 0.4$; D is the van Driest damping function

$$D = 1 - \exp\left(-\frac{y^+}{A^+} \right), \quad A^+ = 26;$$

the vorticity function in the two-dimensional case (the projection of the vector $\mathrm{rot}\,\mathbf{V}$ on the z axis)

$$\Omega = \frac{\partial v}{\partial x} - \frac{\partial u}{\partial y}$$

In the outer layer

$$\mu_{t,out} = K C_{cp} \rho F_{wake} F_{Kleb}(y), \tag{23}$$

where $K = 0.018$, $C_{cp} = 1.6$,

$$F_{Kleb}(y) = \left[1 + 5.5 \left(y \frac{C_{Kleb}}{y_{\max}} \right)^6 \right]^{-1},$$

$$F_{wake} = y_{\max} F_{\max}, \quad F(y) = y|\Omega| D, \quad C_{Kleb} = 0.3, \tag{24}$$

where $y_{\max}$ is determined by the coordinate y, where $F(y)$ reaches its maximum, and $F_{\max} = F(y_{\max})$.

The turbulent viscosity, substituted into equations (10)− (11), is found as follows:

$$\mu_t = \begin{cases} \mu_{t,in}, & y \le y_{cross}, \\ \mu_{t,out}, & y > y_{cross}, \end{cases}$$

where y_{cross} is the coordinate y, at which $\mu_{t,in} = \mu_{t,out}$ the first time as y increases.

Other criteria are also used for the transition from the inner to the outer layer in the hypersonic flow (see, for example, [17, 18]).

We will especially emphasize that the use of algebraic turbulence models in conjunction with the complete Navier − Stokes model faces a number of problems that are not present in the solution of the problem in the classical boundary layer formulation. For example, the choice of boundary layer thickness in a supersonic flow with shock waves is discussed in [18].

5. Results of numerical simulation

The calculated data will be analyzed in the following order. First we make a comparison of the calculated and experimental data. The calculations are performed by correlation relationships and using the NERAT-2D code with two models of turbulent mixing. Then, specific features of the distributions of gas-dynamic functions in the laminar and turbulent boundary layers will be discussed.

In accordance with [1], the following conditions were set in the oncoming stream:

Table 1. Initial data.

Variant # / experiment reference	$\frac{T_w}{T_t}$	M_∞	T_∞ (K)	T_w (K)	ρ_∞ (g/cm^3)	p_∞ (erg/cm^3)	V_∞ (cm/s)
1/[2]	0.2	6	65.04	106.67	1.185×10^{-4}	2.209×10^{4}	9.696×10^{4}
2/[2]	0.6	6	65.04	320.0	1.185×10^{-4}	2.209×10^{4}	9.696×10^{4}
3/[3]	0.65	6	63.01	336.7	1.160×10^{-4}	2.100×10^{4}	9.540×10^{4}
4/[4]	0.11	7.12	240	299	1.120×10^{-4}	7.730×10^{4}	2.210×10^{5}
5/[4]	0.19	8.8	93.99	296.3	2.290×10^{-4}	6.170×10^{4}	1.710×10^{5}
6/[4]	0.26	7.0	105.0	296.0	4.290×10^{-4}	1.290×10^{5}	1.440×10^{5}

The initial data for the calculations were determined from the data of table 1 in [1] (by values M_∞, $T_\infty, \mathrm{Re}_\infty, T_w$) by the successive application of the relations

$$\mu_\infty = 1.458\times10^{-5}\frac{T_\infty^{3/2}}{110.4+T_\infty},\ \text{g/(cm}\times\text{s)},$$

$$a_\infty = \sqrt{\gamma\frac{T_\infty R_0}{M_\Sigma}}\ \text{cm/s},\ R_0 = 8.3145\times10^{7}\ \text{erg/(mole}\times\text{K)},\ \gamma = 1.4,\ M_\Sigma = 29\,\text{g/mole},$$

$$V_\infty = M_\infty a_\infty\ \text{cm/s},\ \rho_\infty = \frac{\mathrm{Re}_\infty\mu_\infty}{\nu_\infty},\ \text{g/cm}^3$$

The braking temperature was estimated from the relationships

$$T_0 = T_\infty + \frac{V_\infty^2}{2c_{p,\infty}},\ c_{p,\infty} = \gamma c_{V,\infty},\ c_{V,\infty} = \frac{R_0}{M_\Sigma(\gamma-1)},\ \mathrm{Re}_\infty = \frac{\rho_\infty V_\infty}{\mu_\infty}\frac{1}{L_{scale}},\ L_{scale} = 100\ \text{cm}$$

For reference, the conditions in the oncoming stream are given in table 2.

Table 2.

Variant	μ_∞ (g/(cm × s))	λ_∞ (erg/(cm × K × s))	Re_∞ (1/cm)
1	0.436×10^{-4}	0.608×10^{3}	2.64×10^{7}
2	0.436×10^{-4}	0.608×10^{3}	2.64×10^{7}
3	0.421×10^{-4}	0.486×10^{3}	2.64×10^{7}
4	0.155×10^{-3}	0.214×10^{4}	1.60×10^{7}
5	0.650×10^{-4}	0.789×10^{3}	6.02×10^{7}
6	0.728×10^{-4}	0.898×10^{3}	8.46×10^{7}

Figure 2 shows the distribution of the Stanton numbers St (8) calculated from the correlations (1), (5), and also using the author's code NERAT-2D with three different numbers $\mathrm{Pr}_t = 0.6$; 0.7 and 1.0. Here we used the Prandtl mixing model. In the case under consideration, $\mathrm{Re}_x = 4\times10^6$ was assumed and the transition from the laminar flow regime to the turbulent flow was assumed to be instantaneous.

We note a good agreement between the calculated densities of convective heat fluxes in both laminar and turbulent flows with experimental data [2]. The effect of the given Pr_t numbers on the density of convective heat fluxes for this variant is insignificant.

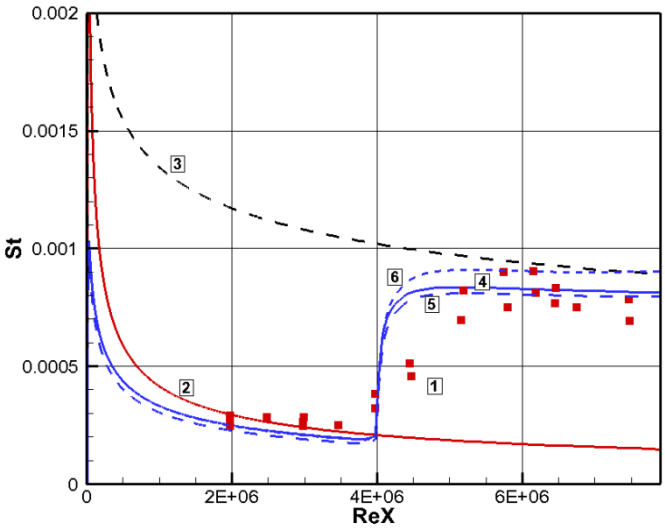

Figure 2. Distribution of the numbers St along the surface of the streamlined plate in the first variant of the calculation: 1 – experiment [2]; 2, 3 – calculation using the correlation relations (1) and (5); 4, 5, 6 – calculations of this work for $\mathrm{Pr}_t = 0.6, 0.7$ and 1.0, respectively (NERAT–2D code with the Prandtl mixing model).

Figure 3 shows similar data for the second variant. The main difference between the 1st and 2nd variants is that in the second case the surface of the plate is noticeably heated, which corresponds more to the actual flight situation of the supersonic apparatus at $\mathrm{M}\sim6$. In the second case, the Pr_t number strongly affects on the heating intensity of plate. As before, the laminar-turbulent transition was not modeled.

Figures 4 and 5 show the results of modeling heat exchange using the Baldwin-Lomax model. Note that for a heated surface this model yields underestimated values of the numbers St at $\mathrm{Pr}_t = 0.72$.

The third variant of calculation is practically similar to the first two (see figures 6 an 7). However, it corresponds to a different series of experiments and a somewhat higher surface temperature. The calculated data in figures 6 show somewhat worse agreement with the experimental data [3] when using both models of turbulent mixing. Note that the calculated data [1] also deviate from these experimental data.

The results of a comparison with the experimental data [4] on heat transfer in the range of Mach numbers $\mathrm{M} = 7 \div 8.8$ are shown in figures 8– 10, respectively, for the calculated cases 4– 6.

In addition to comparing the data on the heating of the streamlined plate (the number St), the available data on the coefficient of surface friction were compared. Figures 11,12 give results of calculating C_f for the first variant by the correlation ratios and by the NERAT-2D code using the Prandtl mixing model and the Baldwin-Lomax model. In figures 13,14 compares analogous data with experiment [3] for the second calculated case using the Prandtl and Baldwin – Lomax models. In general, we note a satisfactory agreement of the calculated data with the correlation data and experiment.

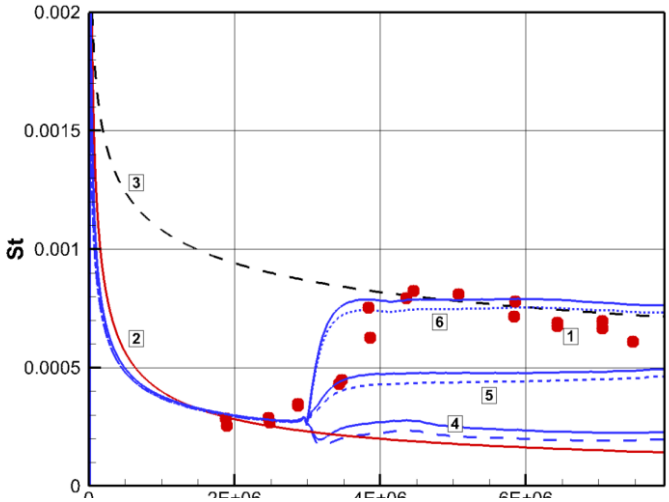

Figure 3. Distribution of the numbers St along the surface of the streamlined plate in the second variant of the calculation: 1 – experiment [2]; 2, 3 – calculation using the correlation relations (1) and (5); 4, 5, 6 – calculations of this work with $\mathrm{Pr}_t = 0.6, 0.7$ and 1.0, respectively (NERAT-2D code with Prandtl mixing model, dushed curves – convective heating, solid curves – with allowance for friction heating).

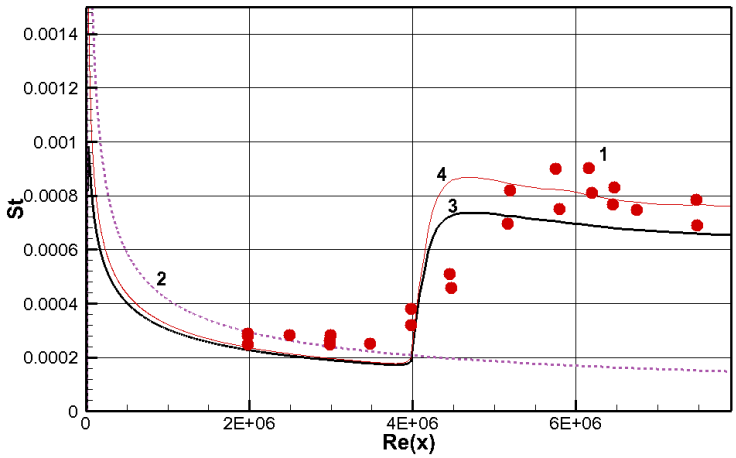

Figure 4. Distribution of the numbers St along the surface of the streamlined plate in the first version of the calculation: 1 – experiment [2]; 2 – calculation using the correlation relations (1) for the laminar boundary layer; 3,4 – calculations of this work using the NERAT–2D code with the Baldwin – Lomax model; 4 – total density of heat flow due to thermal conductivity and friction. $\mathrm{Pr}_t = 0.72$.

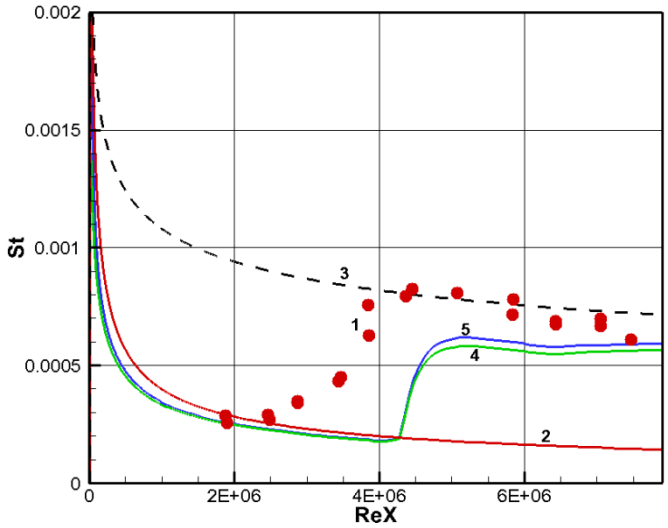

Figure 5. Distribution of the numbers St along the surface of the streamlined plate in the second version of the calculation: 1 – experiment [2]; 2, 3 – calculation using the correlation relations (1) and (5); 4, 5 – calculations of this work using the NERAT–2D code with the Baldwin – Lomax model; 5 is the total density of the heat flux due to thermal conductivity and friction.

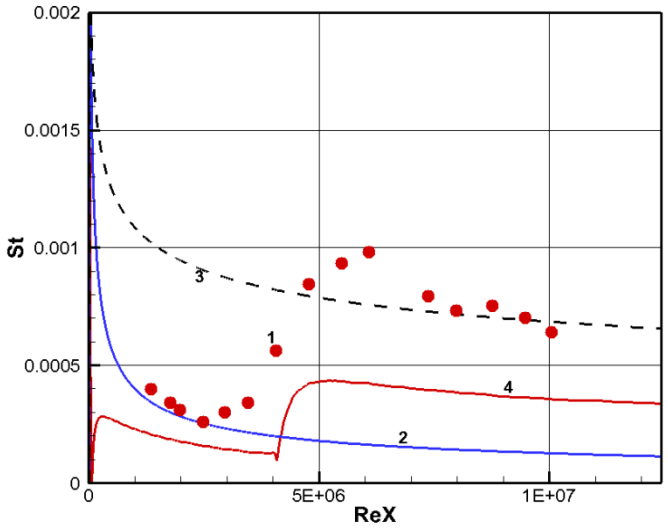

Figure 6. Distribution of the numbers St along the surface of the streamlined plate in the third version of the calculation: 1– experiment [3]; 2, 3 – calculation using correlation ratios for laminar (1) and turbulent (5) boundary layer; 4 – calculations of this work using the NERAT–2D code with the Baldwin – Lomax model. $\mathrm{Pr}_t = 0.72$.

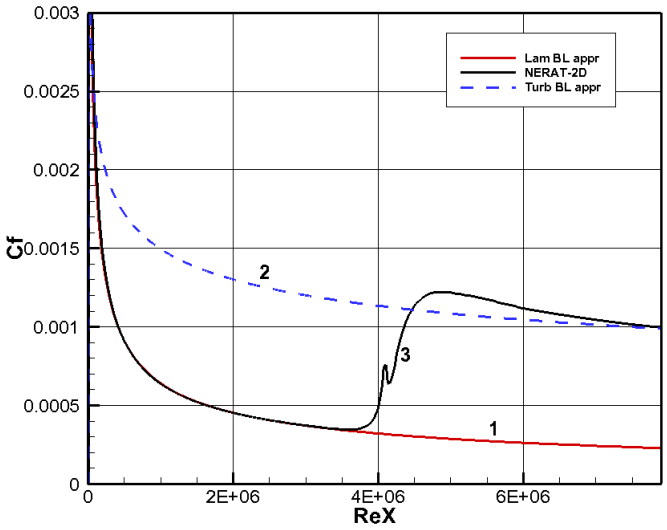

Figure 7. Distribution of the coefficient of surface friction C_f along the surface of the streamlined plate in the third variant of calculation: 1, 2 – calculation using correlation relations for laminar (1) and turbulent (5) boundary layer; 3 – calculations of this work using the NERAT-2D code with the Baldwin – Lomax model. $\mathrm{Pr}_t = 0.72$.

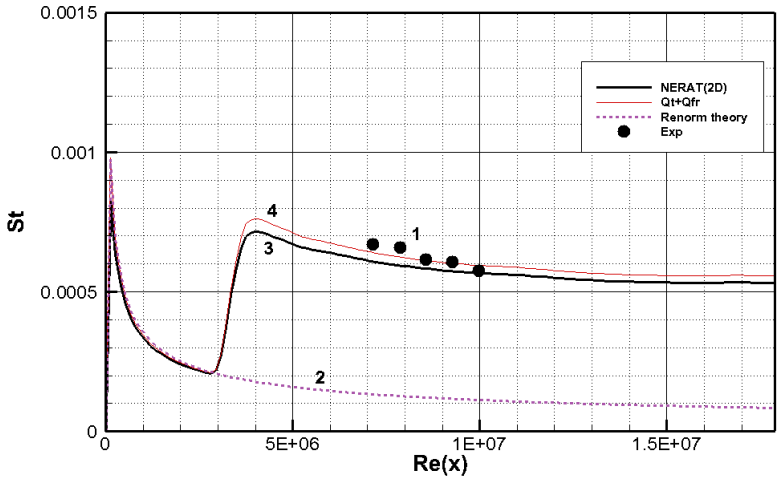

Figure 8. Distribution of the numbers St along the surface of the streamlined plate in the 4th variant of the calculation: 1 – experiment [4]; 2 – calculation using the correlation relations (1) for the laminar boundary layer; 3,4 – calculations of this work using the NERAT-2D convective component code and taking into account the friction heating (4) with the Baldwin – Lomax model. $\mathrm{Pr}_t = 0.7$.

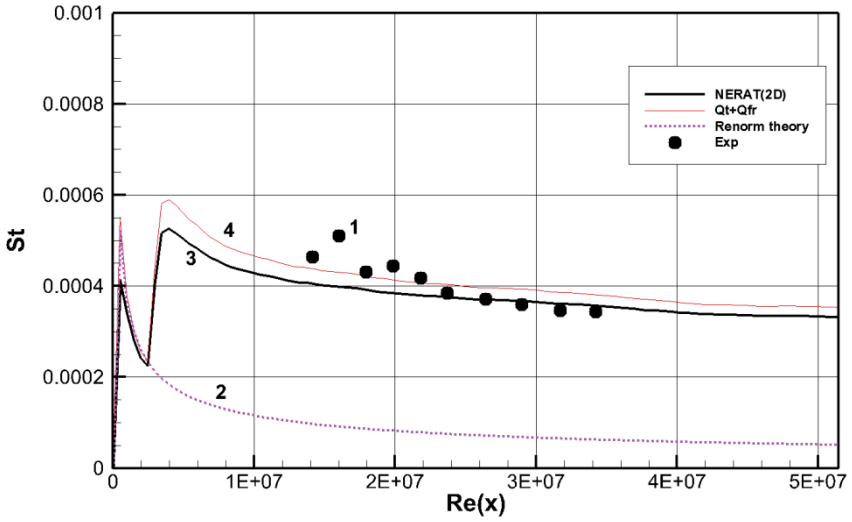

Figure 9. Distribution of the numbers St along the surface of the streamlined plate in the 5th version of the calculation: 1 – experiment [4]; 2 – calculation using the correlation relations (1) for the laminar boundary layer; 3,4 – calculations of this work using the NERAT-2D convective component code and taking into account the heating by the friction with the Baldwin – Lomax model.

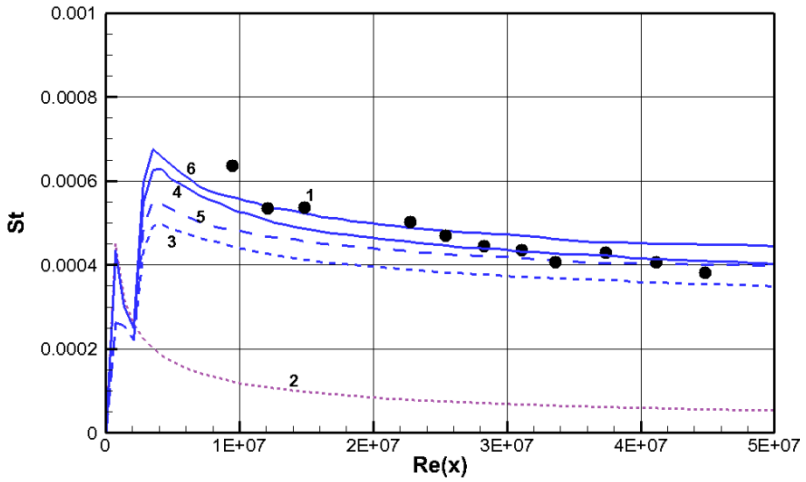

Figure 10. Distribution of the numbers St along the surface of the streamlined plate in the 6th version of the calculation: 1 – experiment [4]; 2 – calculation using the correlation relations (1) for the laminar boundary layer; 3– 6 – calculations of this work using the NERAT-2D convective component (3.5) and taking into account friction heating with the Baldwin – Lomax model (4.6). $\mathrm{Pr}_t = 0.7$ (3.4) and $\mathrm{Pr}_t = 1.0$ (5.6).

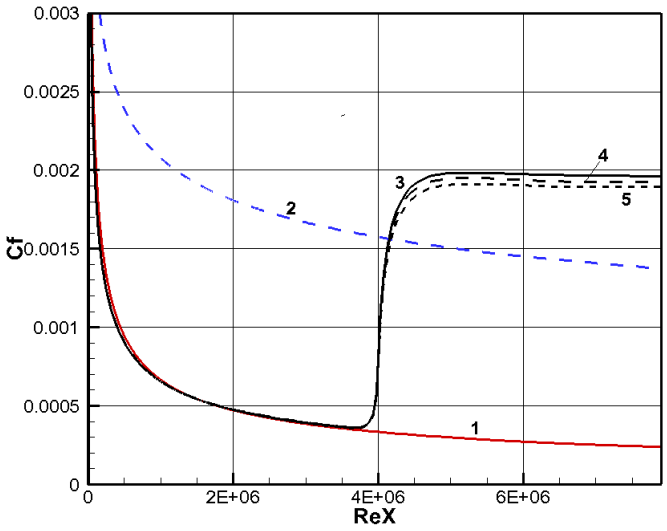

Figure 11. Distribution of the coefficient of surface friction C_f along the surface of the streamlined plate in the first variant of the calculation: 1, 2 – calculation using correlation ratios for laminar (1) and turbulent (5) boundary layer; 3, 4, 5 – calculations of this work using the NERAT-2D code with the Prandtl mixing path model. $\mathrm{Pr}_t = 0.6, 0.72, 1.0$.

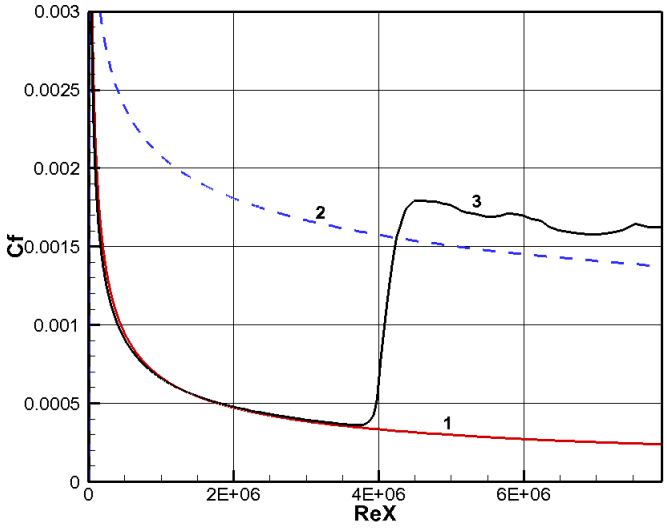

Figure 12. Distribution of the coefficient of surface friction C_f along the surface of the streamlined plate in the first variant of calculation: 1, 2 – calculation using correlation relations for laminar (1) and turbulent (5) boundary layer; 3 – calculations of this work using the NERAT-2D code with the Baldwin – Lomax model. $\mathrm{Pr}_t = 0.72$.

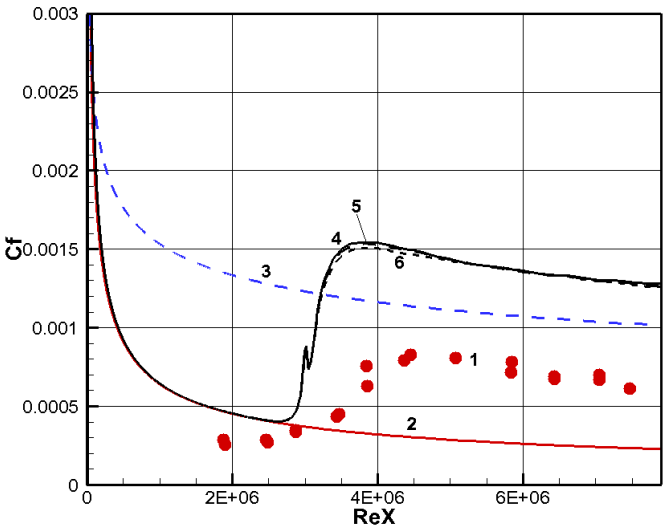

Figure 13. Distribution of the coefficient of surface friction C_f along the surface of the streamlined plate in the second variant of calculation: 1, 2 – calculation using correlation relations for laminar (1) and turbulent (5) boundary layer; 3, 4, 5 – calculations of this work using the NERAT-2D code with the Prandtl mixing path model. $\mathrm{Pr}_t = 0.6, 0.72, 1.0$.

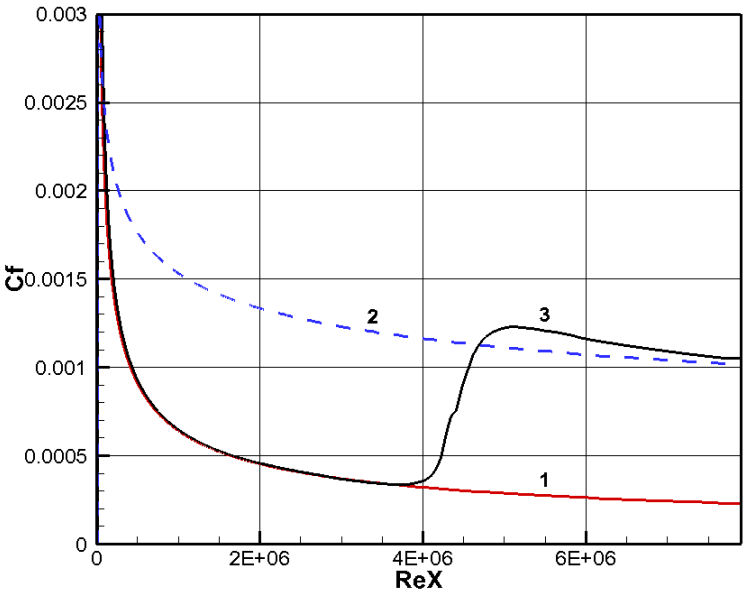

Figure 14. Distribution of the coefficient of surface friction C_f along the surface of the streamlined plate in the second variant of calculation: 1, 2 – calculation using correlation relations for laminar (1) and turbulent (5) boundary layer; 3 – calculations of this work using the NERAT-2D code with the Baldwin – Lomax model. $\mathrm{Pr}_t = 0.72$.

Now let us consider some features of the distribution of gas-dynamic functions. Figure 15 shows a two-dimensional pressure field above the surface of the streamlined plate. Its sharp edge has the coordinate $x_0 = 0.01\,\text{cm}$. The distributions of gas-dynamic functions along the normal to the surface were constructed in sections with coordinates

$$x_1 = 10\,\text{cm},\ x_2 = 18\,\text{cm},\ x_3 = 21\,\text{cm},\ x_4 = 24\,\text{cm},\ x_5 = 27\,\text{cm}.$$

Figures 16, *a*, *b* show temperature distributions in 5 sections along the surface of the plate. The first temperature profile corresponds to the laminar flow regime, and the subsequent 5 distributions correspond to the turbulent boundary layer. Figure 16, *b* shows the same distributions, but closer to the surface. It is clearly seen how the temperature gradients increase in the turbulent boundary layer, and as the displacement along the surface increases, the thickness of the temperature boundary layer increases. In this case, the temperature profiles are similar to the longitudinal velocity distributions (figure 17) with regions of the viscous sub layer, buffer zone, the zone of the developed turbulent boundary layer with a logarithmic velocity distribution and the outer part of the boundary layer well studied in the literature. We note that in this case the highest temperature in the boundary layer slightly exceeds the surface temperature.

Figure 18 shows the profiles of molecular and turbulent viscosity in six sections along the x axis. At $y < 2 < 10^{-2}$ cm, the molecular viscosity prevails in the viscous sub layer, and at large distances from the wall, the turbulent viscosity. In the viscous sub layer the turbulent viscosity $\mu_{t,in}$ is determined by the formula (22), and above the surface by the model $\mu_{t,out}$ (23). Corresponding distributions are shown in figure 19. From the indicated relations it is clear that vortex functions $|\Omega|$ are the determining functions, the profiles of which are shown in figure 20. We note the regions of nonmonotonicity of these functions due to the specific nature of the flow near the shock wave. The profiles of the function $F(y)$ (24), which determines the turbulent viscosity $\mu_{t,out}$ in the Baldwin – Lomax model are shown in figure 21.

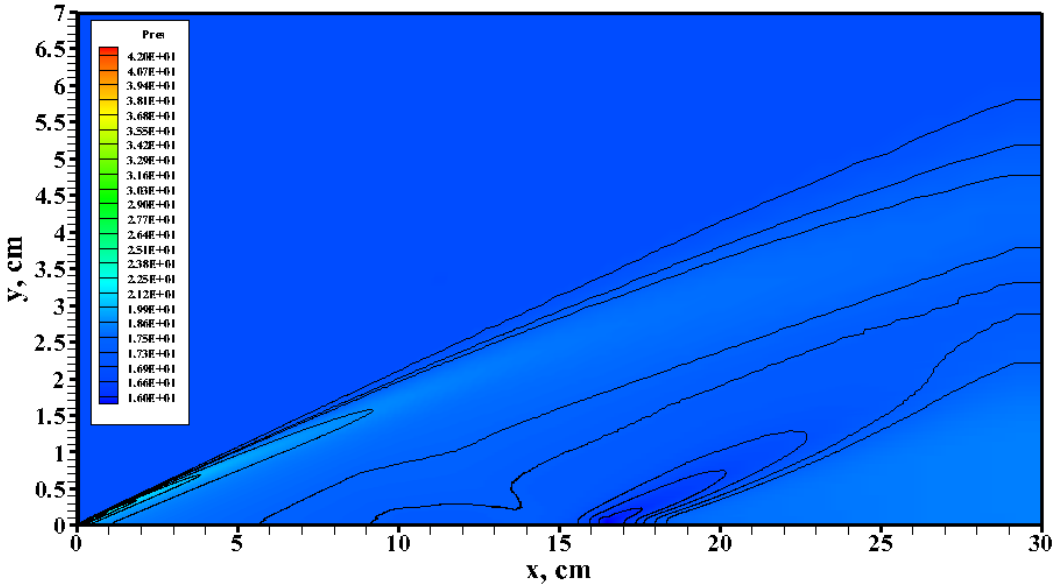

Figure 15. Pressure field above the plate surface for the 2nd variant.

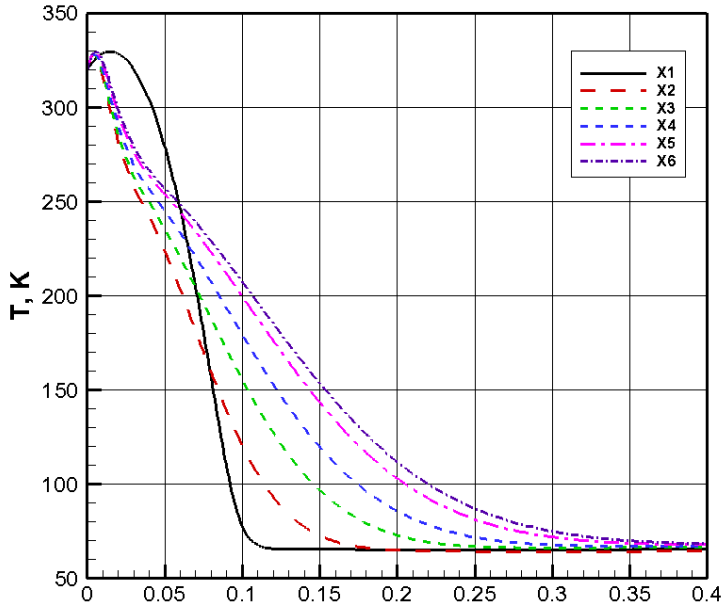

Figure 16, *a*. Temperature distribution along the normal to the surface in 6 sections along the surface of the plate for the 2nd variant. The Baldwin – Lomax model. $\mathrm{Pr}_t = 0.72$.

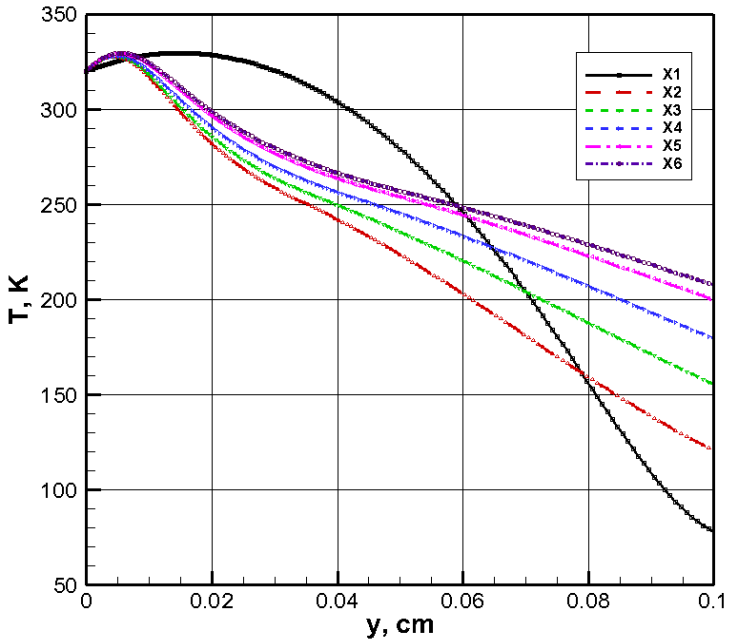

Figure 16, *b*. Temperature distribution along the normal to the surface in 6 sections along the surface of the plate for the 2nd variant. The Baldwin – Lomax model. $\mathrm{Pr}_t = 0.72$.

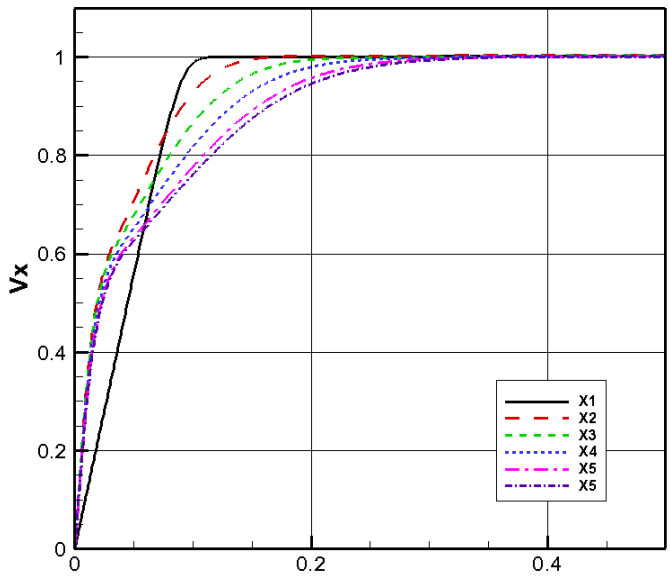

Figure 17. Distribution of longitudinal velocity in a direction normal to the surface in 6 sections along the x axis. The second variant. The Baldwin – Lomax model. $\mathrm{Pr}_t = 0.72$.

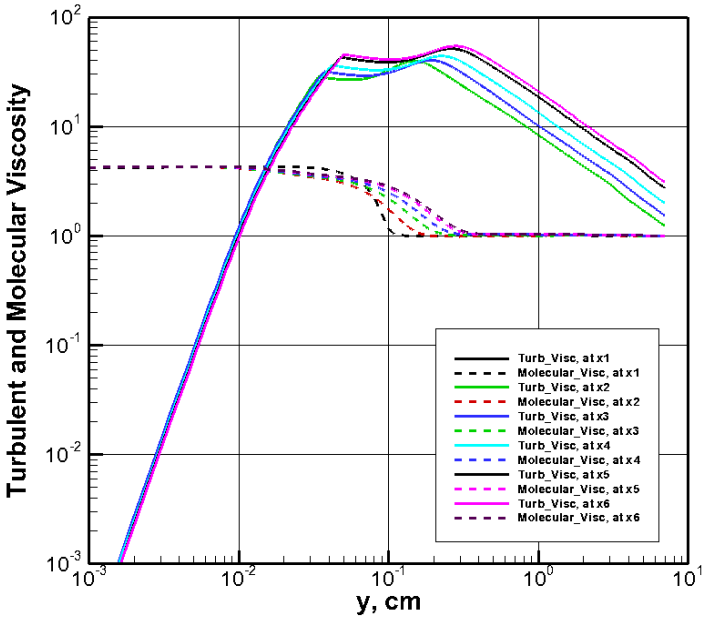

Figure 18. Distributions of the molecular and turbulent viscosity along the normal to the plate in 6 sections with respect to x. The second calculation variant. The Baldwin – Lomax model. $\mathrm{Pr}_t = 0.72$.

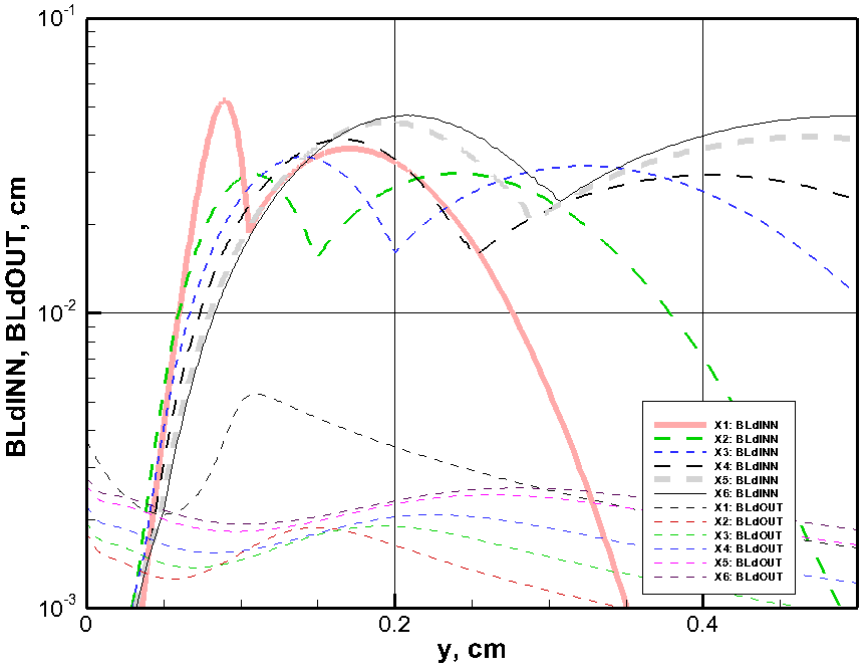

Figure 19. Distributions of two components of turbulent viscosity along the normal to the plate in 6 sections with respect to x. The second calculation variant. The Baldwin – Lomax model. $\mathrm{Pr}_t = 0.72$.

To the question of the difference between the results of modeling of turbulent mixing in the framework of the boundary layer model from the solution of the complete Navier – Stokes equations, we point out the distributions of the normal to surface velocity $V_y = \nu/V_\infty$ in different sections with respect to x and the pressure gradient. Such distributions are shown in figures 22 and 23. Despite the fact that the absolute values of V_y are about 100 times smaller than the characteristic value $V_x = u/V_\infty \approx 1$, it should be taken into account that the derivatives in the outer region can nevertheless be commensurable, which will affect the distribution of the vortex function Ω.

The distributions of the function $y^+(21)$ in different sections along the surface of the plate are shown in figure 24. The smallest value of y^+ near the surface is equal to $y^+_{\min} = 0.3$ cm.

Distributions of similar functions in the boundary layer using the Prandtl mixing length model are shown in figures 25– 31. Note that the data presented in these figures correspond to the case of a cold surface ($T_w/T_t = 0.2$). Particularly noteworthy is the oscillatory character of the behavior of turbulent viscosity (figures 27, 28) and the function $|\Omega|$ (figure 29). The temperature distributions (figure 25), longitudinal (figure 26) and transverse (figure 30) velocities are similar to the previous case.

These oscillations of the vortex function are related to a complex flow over the plate than is modeled in the boundary-layer models. A possible way to deal with these oscillations, which can lead to a general instability of the computational process, can be a limitation of the vortex function from below.

Another feature of the use of the Prandtl mixing length model is the condition (19), which is shown graphically in figure 28. It follows that for $y/\delta > 0.2$ the length of the mixing path remains constant in the outer part of the boundary layer.

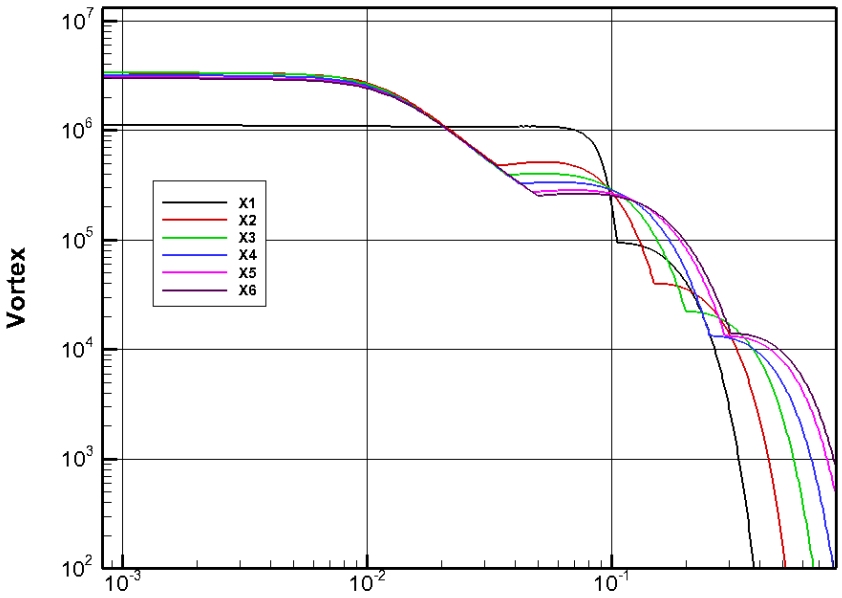

Figure 20. Distributions of the vortex functions along the normal to the plate in 6 sections with respect to x. The second calculation variant. The Baldwin – Lomax model. $\mathrm{Pr}_t = 0.72$.

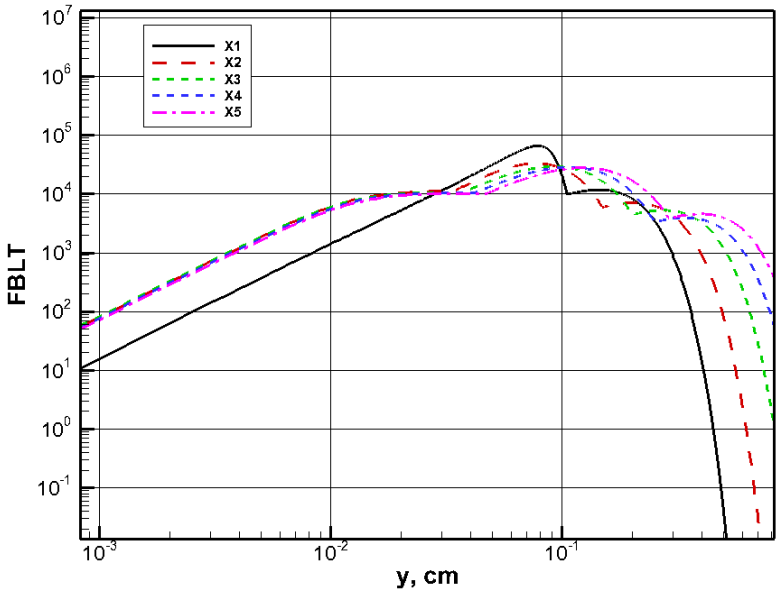

Figure 21. Distributions of functions $F(y) = y|\Omega|D$ along the normal to the plate in 6 sections with respect to x. The second calculation variant. The Baldwin – Lomax model. $\mathrm{Pr}_t = 0.72$.

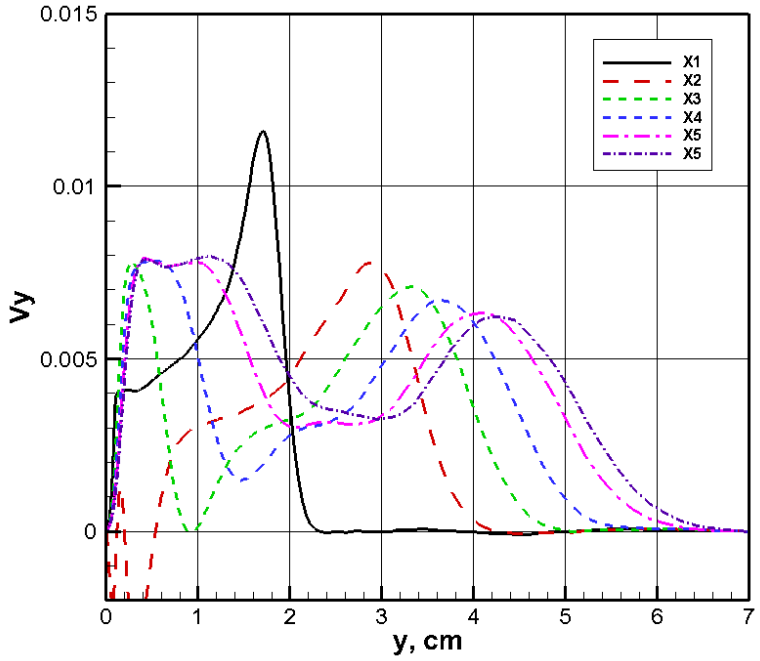

Figure 22. Transverse to the flow velocity $V_y = \nu/V_\infty$ in different sections along the x-axis. The second calculation variant. The Baldwin – Lomax model. $\mathrm{Pr}_t = 0.72$.

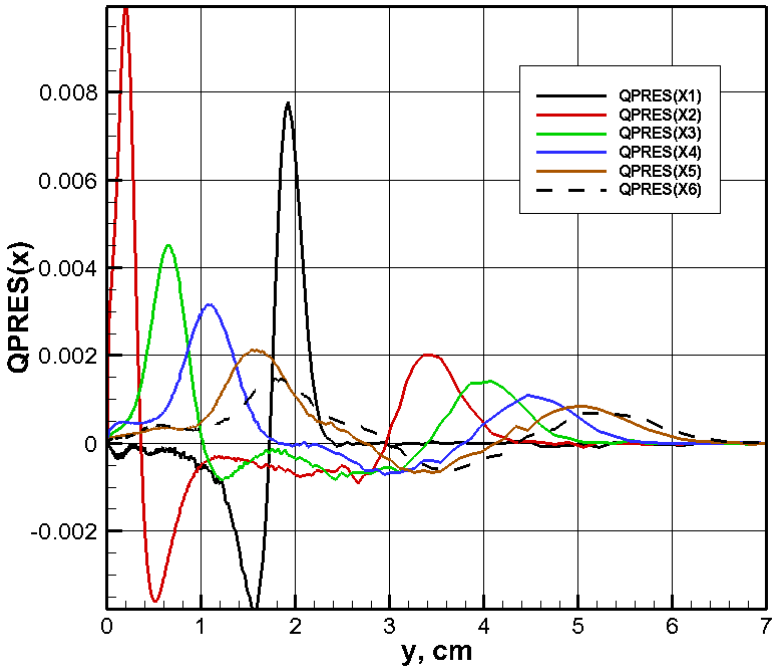

Figure 23. Distribution of functions $\mathrm{grad}(p)$ in different cross-sections along the x-axis The second variant. The Baldwin – Lomax model. $\mathrm{Pr}_t = 0.72$.

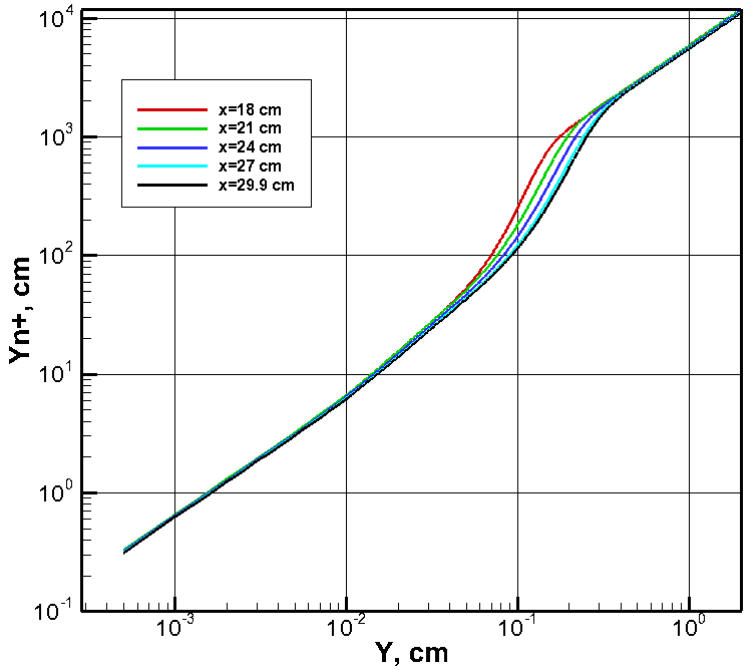

Figure 24. Distribution of functions y^+ in different cross-sections along the x-axis. The second variant. The Baldwin – Lomax model. $\mathrm{Pr}_t = 0.72$.

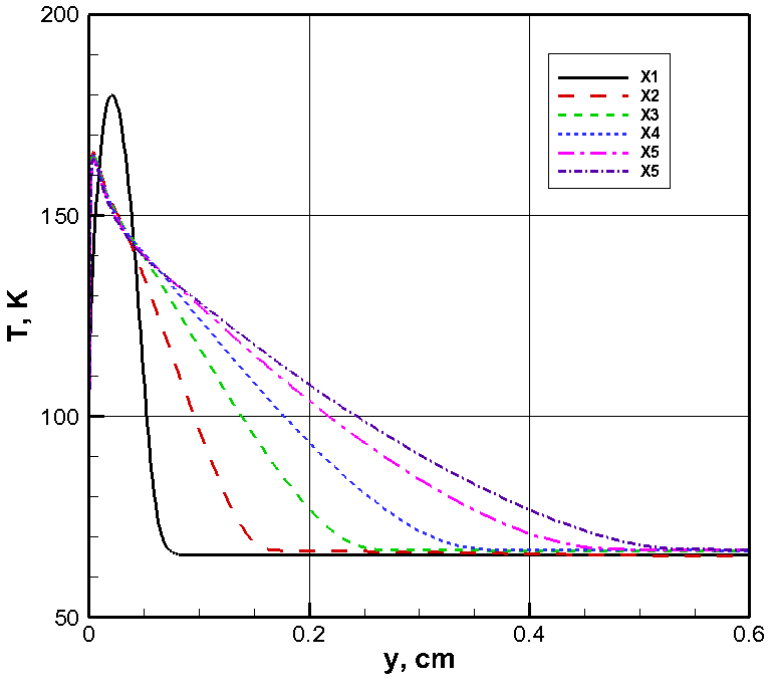

Figure 25. Temperature distribution along the normal to the surface in 6 sections along the surface of the plate for the 1st variant. Model of the Prandtl mixing path. $\mathrm{Pr}_t = 0.6$.

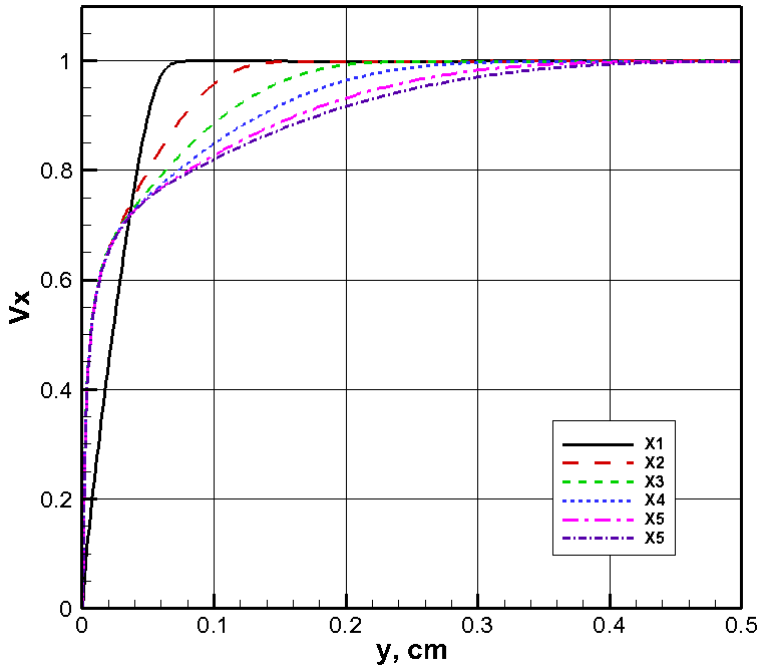

Figure 26. Distribution of longitudinal velocity along the normal to the surface in 6 sections along the surface of the plate for the 1st variant. Model of the Prandtl mixing path. $\mathrm{Pr}_t = 0.6$.

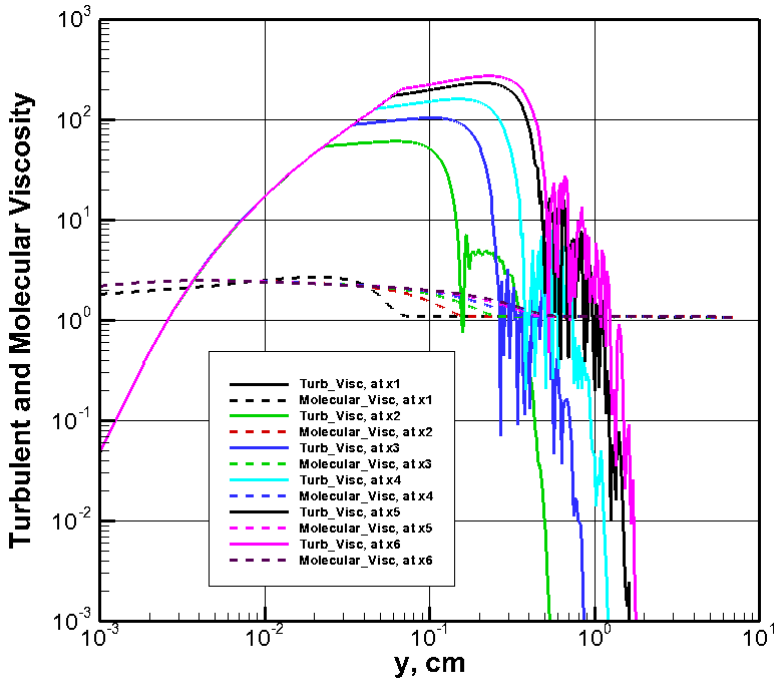

Figure 27. Distribution of turbulent and molecular viscosity along the normal to the surface in 6 sections along the surface of the plate for the first variant. Model of the Prandtl mixing path. $\mathrm{Pr}_t = 0.6$.

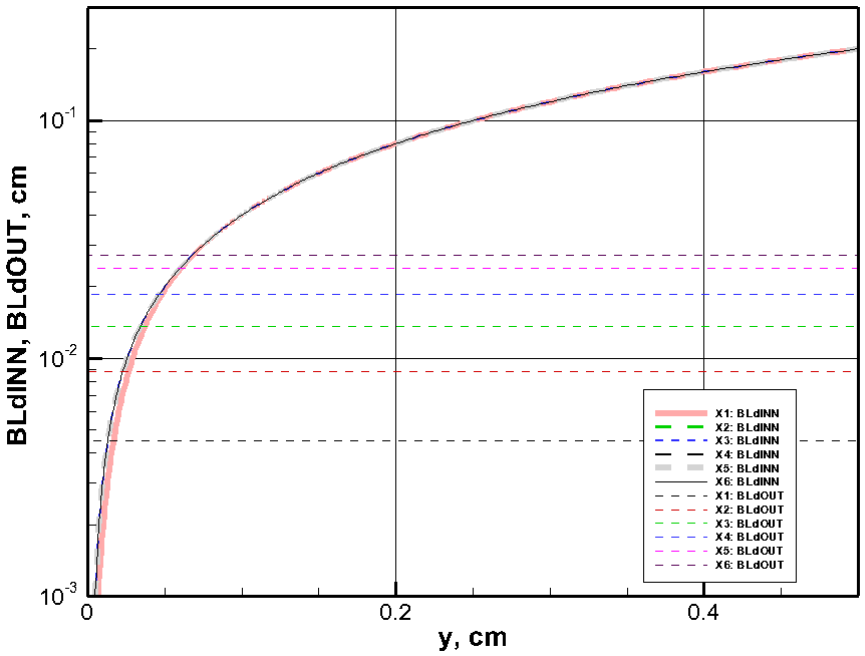

Figure 28. Distribution of functions along the normal to the surface in 6 sections along the surface of the plate for the 1st variant. Model of the Prandtl mixing path. $\mathrm{Pr}_t = 0.6$.

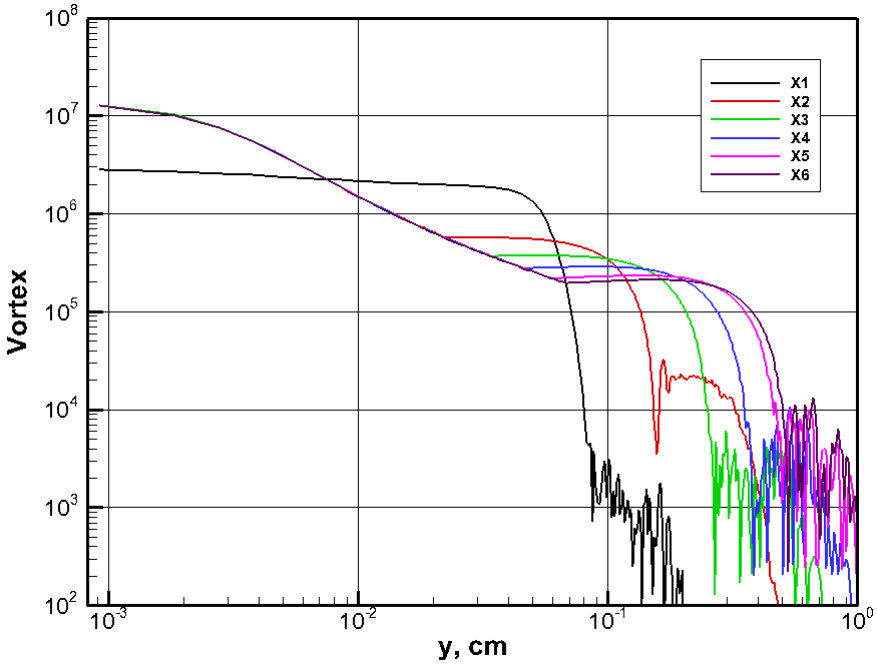

Figure 29. Distribution of the vortex of velocity along the normal to the surface in 6 sections along the surface of the plate for the 1st variant. Model of the Prandtl mixing path. $\mathrm{Pr}_t = 0.6$.

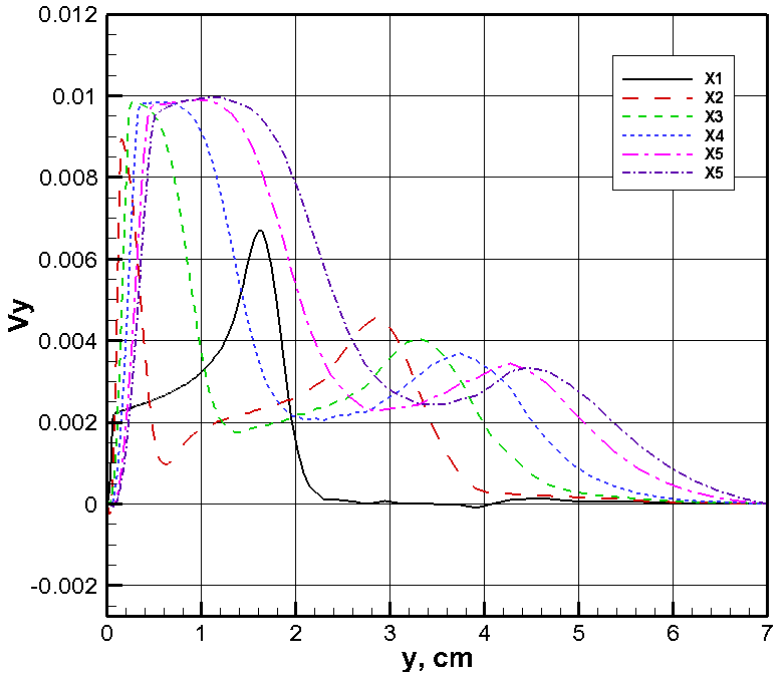

Figure 30. Distribution of the transverse velocity component along the normal to the surface in 6 sections along the surface of the plate for the 1st variant. Model of the Prandtl mixing path. $\mathrm{Pr}_t = 0.6$.

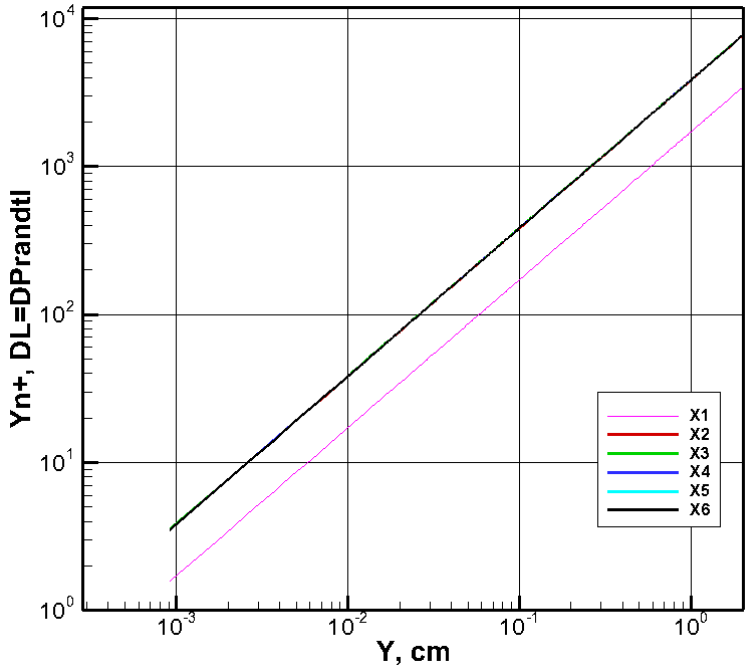

Figure 31. Distribution of the function y^+ along the normal to the surface in 6 sections along the surface of the plate for the 1st variant. Model of the Prandtl mixing path. $\mathrm{Pr}_t = 0.6$.

6. Conclusion

The experimental data on plate heat transfer in supersonic air flows are compared for Mach numbers $M = 6 \div 8.8$ with the calculated data obtained using the Navier – Stokes flow model in conjunction with the analytical models of turbulent mixing of the Prandtl mixing length and the Baldwin-Lomax model. The author's computer code NERAT-2D was used in the calculations. A satisfactory agreement with the experimental data is obtained, which gives grounds for recommending the use of these algebraic turbulent mixing models in conjunction with the Navier – Stokes model for more complex configurations of hypersonic flow, which was also recommended in other papers (see, for example, References 17,18).

Along with this, attention is drawn to the need for accurate application of boundary layer turbulent mixing models to the analysis of complete flow models.

Acknowledgments

The work was performed within the framework of the Government program of basic research of the Russian academy of sciences (contract # AAAA–A17–117021310372–6) and partially under support of the RFBR grant # 016 – 01– 00379.

References

[1] Dilley A D 2001 Evaluation of CFD Turbulent Prediction Techniques and Comparison with Hypersonic Experimental Data *NASA/CR*–2001–210837 26 p
[2] Bertram M H, Cary Jr A M and Whitehead Jr A H 1968 Experiments with Hypersonic Turbulent Boundary Layers on Flat Plate and Delta Wings *AGARD Specialists' Meeting on Hypersonic Boundary Layers and Flow Fields* (London, England)
[3] Bertram M H and Neal Jr L 1965 Recent Experiments in Hypersonic Turbulent Boundary Layer. *AGARD Specialists' Meeting on Recent Developments in Boundary Layer Research* (Italy)
[4] Wallace J E 1967 Hypersonic Turbulent Boundary Layer Studies at Cold Wall Conditions *Proc/ of the 1967 Heat Transfer and Fluid Mechanics Institute* (Stanford University Press) pp 427–451
[5] Walters R W, Reu T, McGrory W D and Hicks J W A 1988 longitudinally Patched Approach with Application to High Speed Flows *AIAA Paper* 88–0715 13 p
[6] Baldwin B S and Lomax H 1978 Thin Layer Approximation and Algebraic Model for Separated Turbulent Flows *AIAA Paper 78–0257* 8p
[7] Surzhikov S T 2013 Convective heating of small-radius spherical blunting for relatively low hypersonic velocities *High Temperature* **51**(2) pp 231–245
[8] Surzhikov S T 2016 Radiative Gas Dynamics of the Fire-II Superorbital Space Vehicle *Technical Physics* **61** (3) pp 349–359
[9] Zemljanskii B A, Lunev V V, Vlasov V I, Gorshkov A B, Zalogin G N, Kovalev R V, Marinin V P and Murzinov I N 2014 *Convective heating of flight crafts*M. (Fizmatlit) 330 p (in Russian)
[10] Tannehill J C, Anderson D A and Pletcher R H 1997*Computational Fluid Mechanics and Heat Transfer* (Taylor & Francis) 792p
[11] Date A W 2005 *Introduction to Computational Fluid Dynamics* (Cambridge University Press) 377p
[12] Cebeci T and Bradshaw P 2012 *Physical and Computational Aspects of Connective Heat Transfer* (Springer–Verlag) 486p
[13] Loitsjansky L G 2003 *Mechanics of Fluids and Gases* (M: "Dropha") 840 p (in Russian)
[14] Horstman C C 1987 Prediction of Hypersonic Shock-Wave/Turbulent-Boundary-Layer Interaction Flows *AIAA 87-1367* 10 p
[15] Shirazi S A and Truman C R 1987 Comparison of Algebraic Turbulence Model for PNS Predictions of Supersonic Flow Past a Sphere-Cone *AIAA 87-0544* 12 p

[16] Shang J S and Scherr S J 1986 Navier – Stockes Solution for a Complete Re–Entry Configuration *J. Aircraft* **23** (12) pp 881–888
[17] Cheatwood F M and Thompson R A 1993 The addition of algebraic turbulence modelling to program LAURA *NASA TM 107 758* 30p
[18] Visbal M and Knight D 1984 The Baldwin – Lomax Turbulence Model for Two-Dimensional Shock-Wave/Boundary-Layer Interaction *AIAA J* **22** (7) pp 921– 928